

## DETECTION OF A LUMINOUS HOT X-RAY CORONA AROUND THE MASSIVE SPIRAL GALAXY NGC266

ÁKOS BOGDÁN<sup>1</sup>, WILLIAM R. FORMAN, RALPH P. KRAFT, AND CHRISTINE JONES

Smithsonian Astrophysical Observatory, 60 Garden Street, Cambridge, MA 02138, USA; abogdan@cfa.harvard.edu

*Draft version July 18, 2018*

### ABSTRACT

The presence of luminous hot X-ray coronae in the dark matter halos of massive spiral galaxies is a basic prediction of galaxy formation models. However, observational evidence for such coronae is very scarce, with the first few examples having only been detected recently. In this paper, we study the large-scale diffuse X-ray emission associated with the massive spiral galaxy NGC266. Using *ROSAT* and *Chandra* X-ray observations we argue that the diffuse emission extends to at least  $\sim 70$  kpc, whereas the bulk of the stellar light is confined to within  $\sim 25$  kpc. Based on X-ray hardness ratios, we find that most of the diffuse emission is released at energies  $\lesssim 1.2$  keV, which indicates that this emission originates from hot X-ray gas. Adopting a realistic gas temperature and metallicity, we derive that in the  $(0.05 - 0.15)r_{200}$  region (where  $r_{200}$  is the virial radius) the bolometric X-ray luminosity of the hot gas is  $(4.3 \pm 0.8) \times 10^{40}$  erg s<sup>-1</sup> and the gas mass is  $(9.1 \pm 0.9) \times 10^9 M_{\odot}$ . These values are comparable to those observed for the two other well-studied X-ray coronae in spiral galaxies, suggesting that the physical properties of such coronae are similar. This detection offers an excellent opportunity for comparison of observations with detailed galaxy formation simulations.

*Subject headings:* galaxies: individual (NGC266) — galaxies: spiral — galaxies: ISM — X-rays: galaxies — X-rays: general — X-rays: ISM

### 1. INTRODUCTION

The existence of gaseous X-ray coronae around massive galaxies was first predicted by White & Rees (1978). Following this work, galaxy formation simulations aimed to characterize such coronae (White & Rees 1991; Toft et al. 2002; Crain et al. 2010; Vogelsberger et al. 2012). The continuous advances in the implemented physics and applied methodology in the simulations led to major revisions in the predicted properties of the coronae. Given the fundamental nature of these coronae and the disagreement between models, the observational characterization of luminous X-ray coronae offers a unique insight to probe the physical processes that influence galaxy formation and evolution.

Although hot gaseous coronae are ubiquitous for massive early-type galaxies (e.g. Forman et al. 1985; O’Sullivan et al. 2001; Bogdán & Gilfanov 2012), these coronae cannot be used to probe structure formation models. On the one hand, the observed coronae around early-type galaxies may not originate from the accretion of primordial gas, but from the merger process and the corresponding starburst. On the other hand, massive early-type galaxies tend to lie in rich environments, and hence the coronal X-ray gas generally cannot be distinguished from the larger-scale emission associated with the group/cluster. Thus, galaxy formation models can be best tested by exploring hot X-ray coronae around massive spiral galaxies.

The hunt for luminous X-ray coronae *beyond* the optical radii of massive spiral galaxies began with *ROSAT* and continued with *Chandra* and *XMM-Newton* observations (e.g. Benson et al. 2000; Rasmussen et al. 2009). However, early studies failed to detect hot coronae

around normal (undisturbed and low star formation rate) spirals, and only upper limits could be derived. Recently, Anderson et al. (2011) detected a luminous X-ray corona around NGC1961, and Dai et al. (2012) found a hot corona around UGC12591. They measured the spectrum of the integrated emission within 40 kpc for NGC1961 and 24 kpc for UGC12591. While the resulting spectra were dominated by the X-ray emission associated with the galaxies, the integrated temperatures ( $0.60^{+0.10}_{-0.09}$  keV and  $0.64 \pm 0.03$  keV) were consistent with the expectations for a hot corona. In Bogdán et al. (2012) we derived the coronal temperatures and metallicities of NGC1961 and NGC6753 beyond their optical radii, specifically in the 23.5 – 70.5 kpc and 22.0 – 66.0 kpc range. In these regions, the gas temperatures are  $0.61^{+0.10}_{-0.13}$  keV for NGC1961 and  $0.69^{+0.06}_{-0.07}$  keV for NGC6753, which are independent of the X-ray emission associated with the stellar body of the galaxies.

At present only three non-starburst spiral galaxies are detected with luminous X-ray coronae. Given the fundamental importance and the extreme rarity of these coronae, it is essential to identify other systems and explore the variations in coronal properties as a function of the host galaxy properties. Characterizing the coronae in a broad sample of galaxies will place stringent constraints on galaxy formation models.

In this paper, we explore the extended X-ray emission associated with NGC266, using *ROSAT* and *Chandra* X-ray observations. NGC266 is a massive spiral galaxy (SB(rs)ab) with a very modest star-formation rate ( $2.4 M_{\odot} \text{ yr}^{-1}$ ), hence its coronal X-ray emission is not dominated by starburst driven winds (Sect. 3.1). NGC266 is the dominant member of a poor group with six additional low-mass galaxies. The galaxy hosts a low-luminosity active galactic nucleus (LLAGN) (Doi et al.

<sup>1</sup>Einstein Fellow

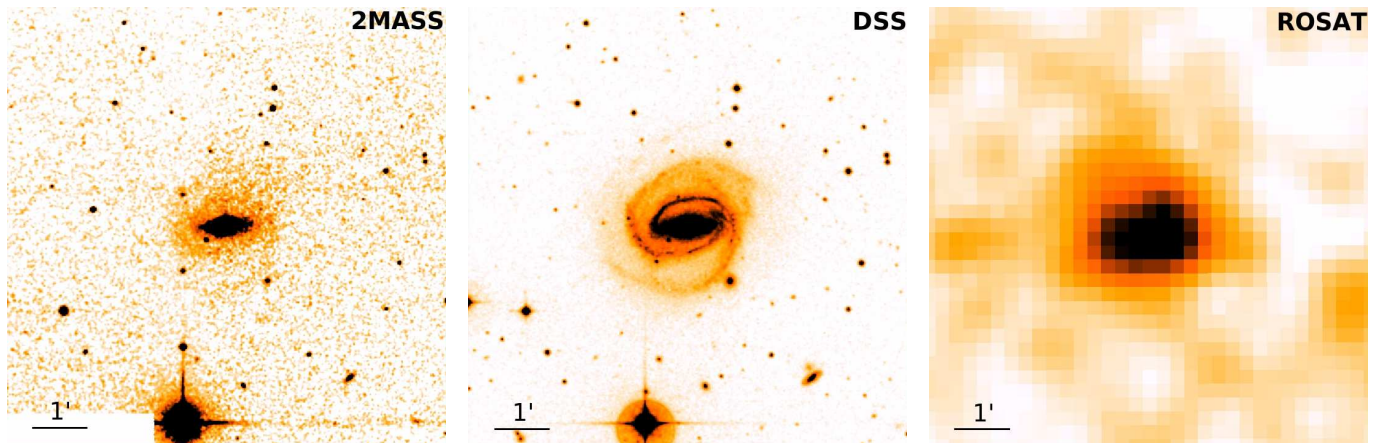


FIG. 1.—  $8' \times 8'$  ( $140 \times 140$  kpc) images of NGC266 at near-infrared, optical, and X-ray wavelengths. The left panel shows the 2MASS K-band image of the galaxy, the middle panel depicts the DSS B-band image, and the right panel shows the  $45''$  Gaussian smoothed  $0.4 - 2.4$  keV band *ROSAT* image. The X-ray emission appears to be more extended than the infrared or optical images of the galaxy, suggesting the presence of a hot X-ray corona in the dark matter halo of NGC266.

2005). For its distance we adopt  $D = 60.3$  Mpc ( $1' = 17.55$  kpc). The Galactic column density towards NGC266 is  $N_{\text{H}} = 5.7 \times 10^{20} \text{ cm}^{-2}$  (Kalberla et al. 2005). Based on the stellar mass of the galaxy and using the results of galaxy formation simulations, the estimated virial mass of NGC266 is  $M_{200} \sim 8 \times 10^{12} M_{\odot}$ , hence its virial radius is  $r_{200} \sim 410$  kpc.

## 2. DATA REDUCTION

### 2.1. *ROSAT*

*ROSAT* observed NGC266 in a pointed PSPC observation on January 3 1992 for 23.4 ks. The data analysis was performed with standard *FTOOLS* packages. Throughout the analysis, we used the  $0.4 - 2.4$  keV data, which offers substantial collecting area, but low instrumental background level. Indeed, the bulk of the *ROSAT* background lies in the  $0.1 - 0.4$  keV band, hence excluding this energy range significantly increases the signal-to-noise ratio for spectra that are not particularly soft. We emphasize that at energies  $< 0.4$  keV, no significant emission is expected from the hot X-ray gas due to the combined effects of the low effective area of *ROSAT* and the rather high Galactic column density.

To study the diffuse emission, we identified and excluded bright point sources. The size of the point source regions were selected to excise  $\gtrsim 95\%$  of the counts. To account for the X-ray emission associated with the LLAGN, we constructed the *ROSAT* PSPC spread function (PSF) distribution using the prescription of Boese et al. (2000). The applied PSF reconstruction is the convolution of five components, whose origin and importance is discussed in Hasinger et al. (1992). According to the in-flight parametrization of the PSF, the analytic PSF distributions offer a robust description of bright point sources at all off-axis radii for energies  $> 0.188$  keV (Hasinger et al. 1992).

To precisely account for all (instrumental and sky) background components, preferably local background regions should be used. Therefore, we employed a circular annulus with  $4 - 8'$  radii around NGC266. Within this region no diffuse emission is detected from the galaxy, and the X-ray emission does not show significant radial variations, making this region suitable to calculate the back-

ground level. Finally, we mention that the vignetting effects were also corrected using the exposure map provided for the specific observation.

### 2.2. *Chandra*

NGC266 was observed by *Chandra* on June 1 2001 (Obs ID: 1610) for 2.0 ks by ACIS-S using a  $1/8$  sub-array configuration with the primary goal to study the LLAGN (Terashima & Wilson 2003). Due to the small image are, these data cannot be used to explore the extended X-ray emitting components of the galaxy.

We analyzed the data with standard CIAO software package tools (CIAO version 4.5; CALDB version 4.5.5.1). The data was reprocessed with the *chandra\_repro* task. To identify bright point sources, we ran the *wavdetect* tool. The source detection sensitivity of the observation is rather high,  $\sim 10^{40} \text{ erg s}^{-1}$ , hence only one point source is resolved at the center of NGC266, which is the LLAGN.

### 2.3. Near-infrared data

We used the K-band images of the Two Micron All Sky Survey (2MASS) to trace the stellar light (Jarrett et al. 2003). Since the 2MASS K-band images of NGC266 are not background subtracted, we used nearby regions away from the galaxy to estimate the background level. Bright foreground stars were visually identified and removed.

## 3. RESULTS

### 3.1. Overall properties of NGC266

We derive the total stellar mass of NGC266 from its K-band luminosity. To derive the K-band luminosity, we rely on the apparent 2MASS K-band magnitude of the galaxy ( $m_K = 8.673$  mag) and use the absolute K-band magnitude of the Sun ( $M_{K,\odot} = 3.28$  mag). The K-band luminosity of NGC266 is  $L_K = 2.5 \times 10^{11} L_{K,\odot}$ . We convert this value to stellar mass using the K-band mass-to-light ratio of  $M_*/L_K = 0.80$ , which we compute from the results of galaxy evolution modeling (Bell et al. 2003) and the  $B - V = 0.82$  color index. Hence, the stellar mass of NGC266 is  $2.0 \times 10^{11} M_{\odot}$ .

The star-formation rate (SFR) of NGC266 is computed from the total infrared luminosity employing the

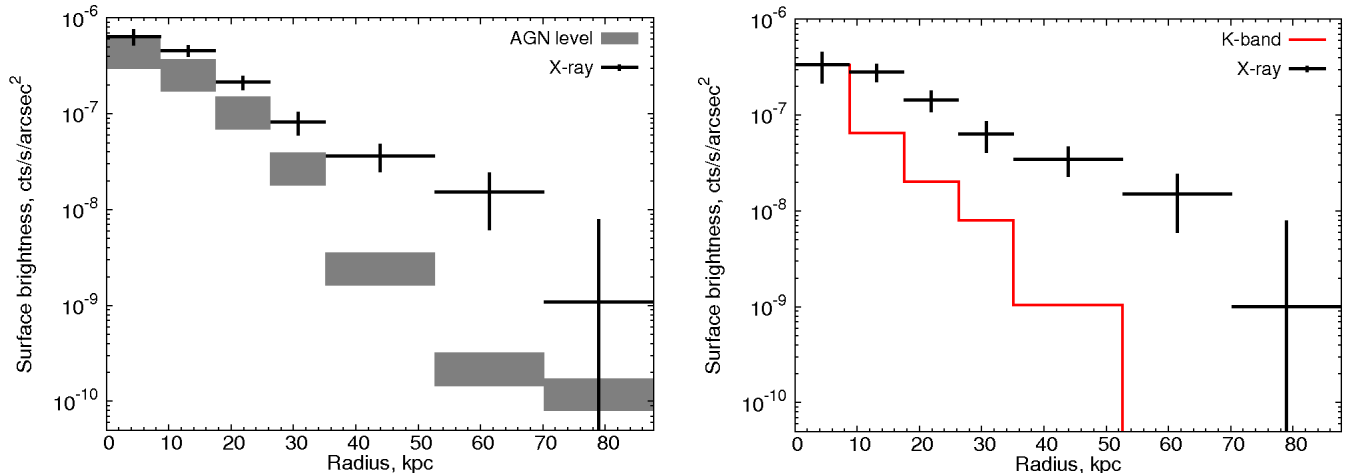


FIG. 2.— *Left*: Surface brightness profile from *ROSAT* data in the 0.4–2.4 keV band using circular annuli. The background components are subtracted, whose level is  $6.3 \times 10^{-8}$  cts  $s^{-1}$  arcsec $^2$ . The shaded area shows the estimated emission associated with the LLAGN. The lower limit of the range assumes that the luminosity of the source remained constant between the *ROSAT* and *Chandra* observations. The upper limit is computed assuming that all counts within  $0.5'$  are associated with the LLAGN. In the  $2 - 4'$  ( $\sim 35 - 70$  kpc) range the contribution of the LLAGN is in the  $\sim 3 - 7\%$  range. *Right*: Same as in the left panel, but the contribution of the LLAGN is subtracted assuming that its luminosity remained constant between the *ROSAT* and *Chandra* observations. The histogram shows the K-band light distribution, which is normalized to the innermost bin. The diffuse X-ray emission extends to at least  $4'$  ( $\sim 70$  kpc), while the bulk of the K-band light is confined to within  $\sim 1.5'$  ( $\sim 26$  kpc).

Kennicutt (1998) relation. To derive the far-infrared fluxes, we follow the methodology of Meurer et al. (1999) and rely on the  $60 \mu\text{m}$  and  $100 \mu\text{m}$  fluxes obtained by the *Infrared Astronomical Satellite*. From the far-infrared luminosity ( $L_{\text{FIR}} = 3.0 \times 10^{43}$  erg  $s^{-1}$ ), we derive the total infrared luminosity ( $L_{\text{TIR}} = 5.3 \times 10^{43}$  erg  $s^{-1}$ ) using the conversion of  $L_{\text{TIR}} = 1.75 L_{\text{FIR}}$  (Calzetti et al. 2000). Hence, the SFR of NGC266 is  $2.4 M_{\odot} \text{ yr}^{-1}$ , which is a rather low value given the stellar mass of the galaxy.

### 3.2. Multi-wavelength images

In Figure 1 we depict an  $8' \times 8'$  ( $140 \times 140$  kpc) region of NGC266 in near-infrared, optical, and X-ray wavelengths. The 2MASS K-band image traces the old stellar population, hence this image highlights the bulge of the galaxy. In the B-band optical image, taken from the Digitized Sky Survey (DSS), the spiral arms are prominent. The image also shows that NGC266 is seen approximately face-on. Both the 2MASS and DSS images indicate the relaxed and undisturbed nature of the galaxy. The right panel shows the 0.4–2.4 keV *ROSAT* image smoothed with a  $45''$  Gaussian kernel. The X-ray image exhibits a bright central region and shows the presence of large-scale extended emission. This emission is more extended than the stellar light, which hints at the presence of a hot X-ray corona surrounding the galaxy. However, NGC266 hosts an LLAGN at its nucleus, whose emission could contribute to the observed diffuse emission due to the broad point spread function (PSF) of *ROSAT*. To assess the importance of the LLAGN in the extended emission, we quantitatively investigate the X-ray and K-band surface brightness distribution of NGC266.

### 3.3. Surface brightness distribution

To study the X-ray emission associated with NGC266, we construct a surface brightness profile from the 0.4–2.4 keV band *ROSAT* image. The profile is extracted from circular annuli centered on the galaxy nucleus. The left

panel of Figure 2 shows the surface brightness profile, which reveals that the diffuse emission extends to at least  $4'$  ( $\sim 70$  kpc). Note that the associated with the LLAGN is not excluded. To estimate the contribution of the LLAGN, we extract the *ROSAT* PSF at 1.1 keV and at  $23'$  off-axis, the approximate location of NGC266. The particular energy choice does not influence our conclusions, since the *ROSAT* PSF is only weakly dependent on the energy (Boese et al. 2000). According to the PSF distribution,  $\sim 95\%$  of the source counts from the LLAGN should be within  $2'$  radius. To estimate the luminosity of the LLAGN, we use two approaches. First, we use the *Chandra* data to derive the expected number of counts detected by *ROSAT*. With the 2 ks *Chandra* exposure we detect 40.5 net counts in the  $0.5 - 8$  keV band, which corresponds to 62.4 *ROSAT* counts in the 0.4–2.4 keV band, if we adopt a power law spectrum with slope of  $\Gamma = 1.4$  and Galactic column density. This method assumes that the luminosity of the LLAGN did not vary between the two observations. However, the X-ray source could have been more luminous at the epoch of the *ROSAT* observation. Hence as a second approach, we assume that all detected *ROSAT* counts within the central  $30''$  are associated with the LLAGN. Under this extreme condition, the point source was  $\sim 2.1$  times brighter, implying that 132.7 *ROSAT* counts are associated with it. Convoluting the number of estimated source counts with the PSF distribution, we show the estimated contribution of the LLAGN to the diffuse emission with shaded area in Figure 2. The profile demonstrates that beyond  $\sim 1.5'$  ( $\sim 26$  kpc), the contribution of the LLAGN does not play a major role. Specifically, in the  $2 - 4'$  ( $\sim 35 - 70$  kpc) region no more than  $\sim 3 - 7\%$  of the detected counts are associated with the bright nuclear source. Thus, the large-scale extended emission around NGC266 cannot be explained by the LLAGN. Moreover, the left panel of Figure 2 demonstrates that the extended emission and the PSF exhibit markedly different distri-

TABLE 1  
THE PARAMETERS OF THE EXTENDED HOT GAS CORONAE IN THE  $(0.05 - 0.15)r_{200}$  RADIAL RANGE.

Galaxy	$L_{0.5-2\text{keV,abs}}$ erg s $^{-1}$	$L_{\text{bol}}$ erg s $^{-1}$	$M_{\text{gas}}$ $M_{\odot}$	$n_e$ cm $^{-3}$	$t_{\text{cool}}$ Gyr
NGC266	$(1.7 \pm 1.3) \times 10^{40}$	$(4.3 \pm 0.8) \times 10^{40}$	$(9.1 \pm 0.9) \times 10^9$	$(4.0 \pm 0.4) \times 10^{-4}$	$38 \pm 4$
NGC1961 $^{\dagger}$	$(2.0 \pm 0.6) \times 10^{40}$	$(5.8 \pm 1.7) \times 10^{40}$	$(1.2 \pm 0.2) \times 10^{10}$	$(3.5 \pm 0.5) \times 10^{-4}$	$45 \pm 6$
NGC6753 $^{\dagger}$	$(2.5 \pm 0.4) \times 10^{40}$	$(6.3 \pm 0.9) \times 10^{40}$	$(1.1 \pm 0.1) \times 10^{10}$	$(3.9 \pm 0.3) \times 10^{-4}$	$51 \pm 4$

$^{\dagger}$  Values taken from Bogdán et al. (2012).

butions, implying that the extended emission cannot be merely attributed to the population of unresolved point sources associated with NGC266.

In the right panel of Figure 2, we show the actual surface brightness profile of the diffuse X-ray emission. From this profile we subtracted the counts associated with the LLAGN, assuming that its luminosity did not change between the *ROSAT* and *Chandra* observations. To trace the stellar light, we extract the radial profile of the 2MASS K-band image using the same annuli as for the X-ray profile. The K-band profile is normalized to match the level of X-ray emission in the innermost bin. As suggested by the images (Figure 1), the surface brightness profile demonstrates that the X-ray light associated with NGC266 extends well beyond the stellar light. While  $\sim 90\%$  of the K-band emission is confined to within  $1.5'$  ( $\sim 26$  kpc), the diffuse X-ray emission extends to at least  $4'$  ( $\sim 70$  kpc), implying that it is not associated with the X-ray emitting components of the stellar body. The radial distribution of the diffuse emission around NGC266 is similar to those obtained in the two other well-studied X-ray coronae in massive spirals (Anderson et al. 2011; Bogdán et al. 2012). To further study the spatial distribution of the diffuse emission, we divided NGC266 into three azimuthal sectors with opening angles of  $120^\circ$ . The azimuthal profiles in the different sectors agree with each other within statistical uncertainties, indicating that the extended emission has a fairly uniform distribution. However, due to the low number of source counts in the outer regions, followup observations are required to map the spatial distribution of the emission in detail.

### 3.4. X-ray hardness ratios

To unveil the nature of the diffuse emission beyond the optical extent of NGC266, it would be desirable to study its X-ray spectrum. However, in the  $2-4'$  region, *ROSAT* only detects  $\sim 40$  net counts, which are not sufficient for spectral analysis. Therefore, we derive X-ray hardness ratios that could differentiate between the two potential origins of the emission: (i) hot gaseous X-ray corona in the dark matter halo of NGC266, or (ii) a multitude of unresolved point sources, presumably originating from (background) AGN. Defining the hardness ratio (HR) as the ratio of net counts  $(1.2-2.4 \text{ keV})/(0.4-1.2 \text{ keV})$ , we expect very different HRs in the two scenarios. Assuming a thermal spectrum with  $kT = 0.6$  keV, a metallicity of 0.2 Solar, and Galactic column density, we expect  $\text{HR} = 0.13$ . Note that such a spectrum was observed for the X-ray coronae of NGC1961 and NGC6753 (Bogdán et al. 2012). If (background) AGN dominate, whose spectrum can be described with a power law model with slope of  $\Gamma = 1.4$  and Galactic column density, we expect  $\text{HR} =$

0.64.

Within the central  $2'$  region, we obtain  $\text{HR} = 0.78 \pm 0.14$ , which is in good agreement with a hard power law spectrum. Indeed, the central region is dominated by the LLAGN, while the population of unresolved LMXB and HMXBs also plays a role. Their spectra can be described with similar power law models. In the  $2-4'$  region, where the contribution of stellar light and the LLAGN is negligible, we obtain  $\text{HR} = 0.20 \pm 0.18$ . This indicates that the emission most likely originates from a soft X-ray emitting component, and this value is consistent with a hot gaseous emission with a temperature less than 1 keV. However, given the large statistical uncertainties, the contribution of a harder component, for example a population of unresolved cosmic X-ray background sources, cannot be excluded. Nevertheless, the X-ray hardness ratios indicate that the bulk of the diffuse emission beyond the stellar body of NGC266 is consistent with that from a gaseous X-ray corona.

### 3.5. Estimated gas parameters

Measuring the properties of the hot X-ray gas in the dark matter halos of massive spirals can place major constraints on galaxy formation models, hence on the physical processes that influence galaxy evolution. To facilitate these efforts, we also derive the gas parameters for NGC266. Since accurate X-ray determinations of the temperature and metallicity are not feasible, we adopt gas parameters, which were measured for the hot X-ray coronae around NGC1961 and NGC6753 (Bogdán et al. 2012). Namely, we assume a gas temperature of  $kT = 0.6$  keV and a metallicity of 0.2 Solar.

We compute the gas parameters in the  $(0.05-0.15)r_{200}$  region, which corresponds to an annulus from  $1.17 - 3.5'$  ( $\sim 20.5 - 61.5$  kpc). Within this region we detect  $79.0 \pm 13.9$  net counts after accounting for the emission associated with the LLAGN. In this computation we assumed that the luminosity of the LLAGN did not change between the *ROSAT* and *Chandra* observations. Assuming the above-described thermal spectrum, the detected counts correspond to an absorbed  $0.5 - 2$  keV luminosity of  $L_{0.5-2\text{keV,abs}} = (1.7 \pm 0.3) \times 10^{40}$  erg s $^{-1}$ . The bolometric luminosity of the gas in the  $(0.05 - 0.15)r_{200}$  region is  $L_{\text{bol}} = (4.3 \pm 0.8) \times 10^{40}$  erg s $^{-1}$ . Using the volume from which the source flux is extracted and assuming that the emission can be described with a thermal plasma emission model (APEC in XSPEC), we estimate that the mean electron density of the gas is  $n_e = (4.0 \pm 0.4) \times 10^{-4}$  cm $^{-3}$ . Assuming a volume filling factor of unity and a constant gas density, the total gas mass is  $M_{\text{gas}} = (9.1 \pm 0.9) \times 10^9 M_{\odot}$ . The cooling time of the gas is estimated from  $t_{\text{cool}} = (3kT)/(n_e\Lambda(T))$ , where

$\Lambda(T)$  is the cooling function, and we obtain  $t_{\text{cool}} = 38 \pm 4$  Gyrs. These values are listed in Table 1, where we also include the gas parameters derived for NGC1961 and NGC6753. The comparison reveals that the gas parameters are similar in all three galaxies.

#### 4. DISCUSSION

Following Bogdán et al. (2012) we investigate if starburst driven winds could be responsible for the observed extended emission around NGC266. According to theoretical considerations, extraplanar X-ray emission driven by starburst winds is expected if the area specific supernova (SN) rate is  $\gtrsim 25 \text{ SN Myr}^{-1} \text{ kpc}^{-2}$  (Strickland et al. 2004). We derive the SN rate from the total far-infrared luminosity  $R_{\text{SN}} = 0.2 L_{\text{FIR}} 10^{11} L_{\odot}$  (Heckman et al. 1990), and obtain  $R_{\text{SN}} = 0.015 \text{ yr}^{-1}$ . Based on this value and the size of the  $D_{25}$  major axis diameter, the area specific SN rate of NGC266 is  $\sim 5.7 \text{ SN Myr}^{-1} \text{ kpc}^{-2}$ , which falls short of the critical value. Thus, NGC266 is unlikely to drive starburst winds at the present epoch.

The detection of a luminous X-ray corona around NGC266 raises the question if other coronae could be detected based on archival *ROSAT* data. In principle, further detections are feasible with *ROSAT*, provided that sufficiently deep pointed observations are available. However, in the local Universe ( $\lesssim 100$  Mpc) most massive normal spiral galaxies were only observed with the *ROSAT* All Sky Survey or with short pointed PSPC observations, which data are not suitable for detailed analysis. Therefore, to extend the sample of massive spirals with luminous coronae, observations with present-day X-ray telescopes are indispensable.

While the present data demonstrate the presence of an extended X-ray emitting component around NGC266, a moderately deep *Chandra* observation could achieve the following goals: (i) conclusively determine the nature of

the extended emission; (ii) assess the X-ray luminosity of the LLAGN; (iii) measure the gas temperature and metallicity, and hence derive accurate gas parameters; (iv) build a precise radial profile, and hence estimate the total confined gas mass, and compute the baryon budget of the galaxy.

NGC266 is the fourth spiral galaxy with a luminous X-ray corona detected beyond its optical radius. Although the increasing number of detections is encouraging, the present sample does not yet allow us to draw general conclusions about the properties of X-ray coronae. The detected galaxies have a narrow range of stellar masses. Therefore, it is essential to characterize the presently detected coronae in more detail and to explore further – preferably lower mass – galaxies. At present, galaxy formation simulations are fairly mature, incorporating supernova and AGN feedback, setting the stage to confront the observations with realistic simulations. Such comparisons offer a unique possibility to constrain the physical processes, in particular the feedback effects, that play a crucial role in the evolution of galaxies from high redshifts to the present-day Universe.

We thank the anonymous referee for helpful comments. ÁB thanks Alexey Vikhlinin for helpful discussions about the *ROSAT* PSF. This research has made use of *Chandra* data provided by the CXC. This publication makes use of data products from the 2MASS, which is a joint project of the University of Massachusetts and the Infrared Processing and Analysis Center/California Institute of Technology, funded by NASA and NSF. The authors acknowledge the usage of the HyperLeda database. ÁB acknowledges support provided by NASA through Einstein Postdoctoral Fellowship grant number PF1-120081 awarded by the CXC, which is operated by the Smithsonian Astrophysical Observatory for NASA under contract NAS8-03060. WF and CJ acknowledge support from the Smithsonian Institution.

#### REFERENCES

- Anderson, M. E. & Bregman, J. N., 2011, *ApJ*, 737, 22  
 Bell, E. F., McIntosh, D. H., Katz, N. & Weinberg, M. D., 2003, *ApJS*, 149, 289  
 Benson, A. J., Bower, R. G., Frenk, C. S. & White, S. D. M., 2000, *MNRAS*, 314, 557  
 Boese, F. G., 2000, *A&AS*, 141, 507  
 Bogdán, Á. & Gilfanov, M., 2011, *MNRAS*, 418, 1901  
 Bogdán, Ákos, Forman, W. R., Vogelsberger, M., et al., 2012, arXiv:1212.0541  
 Calzetti, D., Armus, L., Bohlin, R. C., et al., 2000, *ApJ*, 533, 682  
 Crain, R. A., McCarthy, I. G., Frenk, C. S., Theuns, T. & Schaye, J., 2010, *MNRAS*, 407, 1403  
 Dai, X., Anderson, M. E., Bregman, J. N. & Miller, J. M., 2012, *ApJ*, 755, 107  
 Doi, A., Kameno, S. & Inoue, M., 2005, *MNRAS*, 360, 119  
 Forman, W., Jones, C. & Tucker, W., 1985, *ApJ*, 293, 102  
 Hasinger, G., Turner, T. J., George, I.M., & Boese, G., 1992, *Legacy*, 2, 77  
 Heckman, T. M., Armus, L. & Miley, G. K., 1990, *ApJS*, 74, 833  
 Jarrett, T. H., Chester, T., Cutri, R., Schneider, S. E. & Huchra, J. P., 2003, *AJ*, 125, 525  
 Kalberla, P. M. W., Burton, W. B., Hartmann, D., et al., 2005, *A&A*, 440, 775  
 Kennicutt, R. C. Jr., 1998, *ARA&A*, 36, 189  
 Meurer, G. R., Heckman, T. M. & Calzetti, D., 1999, *ApJ*, 521, 64  
 O’Sullivan, E., Forbes, D. A. & Ponman, T. J., 2001, *MNRAS*, 328, 461  
 Rasmussen, J., Sommer-Larsen, J., Pedersen, K., et al., 2009, *ApJ*, 697, 79  
 Strickland, D. K., Heckman, T. M., Colbert, E. J. M., Hoopes, C. G. & Weaver, K. A., 2004, *ApJ*, 606, 829  
 Terashima, Y. & Wilson, A. S., 2003, *ApJ*, 583, 145  
 Toft, S., Rasmussen, J., Sommer-Larsen, J., Pedersen, K., 2002, *MNRAS*, 335, 799  
 Vogelsberger, M., Sijacki, D., Keres, D., Springel, V. & Hernquist, L., 2012, *MNRAS*, 425, 3024  
 White, S. D. M. & Frenk, C. S., 1991, *ApJ*, 379, 52  
 White, S. D. M. & Rees, M. J., 1978, *MNRAS*, 183, 341